Inorg. Chem. **2008**, *47*, 10372−10377

Favorable Hydrogen Storage Properties of M(HBTC)(4,4′-bipy)·3DMF (M = Ni and Co)

Yaoqi Li,[†] Lei Xie,[†] Yang Liu,[†] Rong Yang,[†] and Xingguo Li*[,†,‡]

Beijing National Laboratory for Molecular Sciences (BNLMS), The State Key Laboratory of Rare Earth Materials Chemistry and Applications, College of Chemistry and Molecular Engineering, Peking University, Beijing, 100871, China, and College of Engineering, Peking University, Beijing, 100871, China

Received May 20, 2008

Two metal−organic frameworks of M(HBTC)(4,4′-bipy)·3DMF (M = Ni and Co; H_3BTC = 1,3,5-benzenetricarboxylic acid; 4,4′-bipy = 4,4′-bipyridine; DMF = N,N′-dimethylformamide) were synthesized by a one-pot solution reaction and a solvothermal method, respectively. The as-prepared samples have high specific surface areas of 1590 m^2/g and 887 m^2/g. The activation at different temperatures for the guest removal prior to gas loading obviously affects the gas sorption process. Ni(HBTC)(4,4′-bipy)·3DMF shows high hydrogen storage capacities of 1.20 wt % at room temperature and 3.42 wt % at 77 K. Co(HBTC)(4,4′-bipy)·3DMF shows capacities of 0.96 wt % at 298 K and 2.05 wt % at 77 K. The hydrogen adsorption heats in the two compounds decrease slightly as a function of the amount adsorbed, and it confirms that the H_2 molecules are combined with stronger sites preferentially. Research on the kinetics of hydrogen adsorption shows a fast saturation process (80 s) and no obvious capacity loss after 20 cycles.

Introduction

Nowadays, worldwide interest is focused on using a clean-burning substitute such as hydrogen in place of fossil fuels, due to both economic and environmental reasons. The storage of this lightweight fuel is one of the most important challenges impeding its practical application, which calls for storing and releasing hydrogen in the proper capacity and condition with fast kinetics and favorable reversibility.[1,2] Physisorption on large surface area materials is one significant approach for storing hydrogen. Some metal−organic frameworks (MOFs) show promising results for hydrogen adsorption at low temperatures under appropriate pressures.[3−9] Compared with other microporous materials such as zeolites and active carbon, the low framework density, the high specific surface area, and especially the controllable crystal structure have made MOFs a favorable research subject.[6,9−21] By crystal engineering,[22] both the pore size[19] and the electronic and chemical nature of the interior surface, on which H_2 molecules will be adsorbed, can be modified by careful designs.

Researchers have proposed that, besides the size and the chemical nature of the porous framework, the rolling surface of the pores and the nonlinearity of the channels may affect the hydrogen uptake properties of MOFs.[14,23,24] To investigate the effects of the rolling surface and nonlinearity on hydrogen adsorption properties, it is necessary to develop hydrogen storage properties in MOFs with differently shaped channels besides normal rectangle channels. The recently

* Author to whom correspondence should be addressed. E-mail: xgli@pku.edu.cn.
† College of Chemistry and Molecular Engineering.
‡ College of Engineering.

(1) Schlapbach, L.; Zuttel, A. *Nature* **2001**, *414*, 353–358.
(2) Grochala, W.; Edwards, P. P. *Chem. Rev.* **2004**, *104*, 1283–1315.
(3) Latroche, M.; Surble, S.; Serre, C.; Mellot-Draznieks, C.; Llewellyn, P. L.; Lee, J. H.; Chang, J. S.; Jhung, S. H.; Ferey, G. *Angew. Chem., Int. Ed.* **2006**, *45*, 8227–8231.
(4) Wong-Foy, A. G.; Matzger, A. J.; Yaghi, O. M. *J. Am. Chem. Soc.* **2006**, *128*, 3494–3495.
(5) Panella, B.; Hirscher, M.; Putter, H.; Muller, U. *Adv. Funct. Mater.* **2006**, *16*, 520–524.
(6) Dinca, M.; Dailly, A.; Liu, Y.; Brown, C. M.; Neumann, D. A.; Long, J. R. *J. Am. Chem. Soc.* **2006**, *128*, 16876–16883.
(7) Lin, X.; Jia, J. H.; Zhao, X. B.; Thomas, K. M.; Blake, A. J.; Walker, G. S.; Champness, N. R.; Hubberstey, P.; Schroder, M. *Angew. Chem., Int. Ed.* **2006**, *45*, 7358–7364.
(8) Loiseau, T.; Lecroq, L.; Volkringer, C.; Marrot, J.; Ferey, G.; Haouas, M.; Taulelle, F.; Bourrelly, S.; Llewellyn, P. L.; Latroche, M. *J. Am. Chem. Soc.* **2006**, *128*, 10223–10230.
(9) Surble, S.; Millange, F.; Serre, C.; Duren, T.; Latroche, M.; Bourrelly, S.; Llewellyn, P. L.; Ferey, G. *J. Am. Chem. Soc.* **2006**, *128*, 14889–14896.

10.1021/ic800919k CCC: $40.75
Published on Web 10/15/2008

solvothermally synthesized MOF,[25] Ni(HBTC)(4,4′-bipy)·3DMF, has a special porous structure with unusual honeycomb channels. For the hydrogen storage of MOFs, it is significant to raise the specific surface areas and the output by facile synthesis methods. Compared with solvothermal methods,[25] the facile one-pot solution assembly method in this work resulted in a shorter reaction time, higher specific surface area, and larger quantity of Ni(HBTC)(4,4′-bipy)·3DMF. In addition, the new MOF of Co(HBTC)(4,4′-bipy)·3DMF was first synthesized to investigate the effects of different metal elements on the hydrogen sorption properties of M(HBTC)(4,4′-bipy)·3DMF. It is for the first time that these M(HBTC)(4,4′-bipy)·3DMF (M = Ni and Co) with particular honeycomb-like channels have been investigated for hydrogen adsorption properties at different temperatures (77, 90, 98, and 298 K). Furthermore, for the understanding of the interaction between H_2 and the special framework, the adsorption heats were calculated for both Ni(HBTC)(4,4′-bipy)·3DMF and Co(HBTC)(4,4′-bipy)·3DMF. The kinetic properties and the reversibility were measured. The effects of porous structure with unusual honeycomb channels and metal sites on the hydrogen sorption properties were also discussed.

Experimental Section

Ni(HBTC)(4,4′-bipy)·3DMF was prepared by a mild solution method. A solution of H_3BTC (H_3BTC = 1,3,5-benzenetricarboxylic acid; 0.211 g, 1.0×10^{-3} mol), 4,4′-bipy (4,4′-bipy = 4,4′-bipyridine; 0.192 g, 1.0×10^{-3} mol), and $Ni(NO_3)_2 \cdot 6H_2O$ (0.292 g, 1.0×10^{-3} mol) in 40 mL of DMF (DMF = N,N′-dimethylformamide) was kept in a glass conical flask and heated at 393 K for 4 h. After being filtered and thoroughly washed by DMF and C_2H_5OH, the obtained green crystals were dried in the air at 333 K for 12 h before other measurements. The yield of Ni(HBTC)(4,4′-bipy)·3DMF was 73%.

Co(HBTC)(4,4′-bipy)·3DMF was prepared by a solvothermal method. A solution of H_3BTC (0.211 g, 1.0×10^{-3} mol), 4,4′-bipy (0.192 g, 1.0×10^{-3} mol), and $Co(NO_3)_2 \cdot 6H_2O$ (0.291 g, 1.0×10^{-3} mol) in 20 mL of DMF was sealed in a 25 mL Teflon-lined autoclave and heated at 353 K for 72 h. The resultant red powders were washed with DMF and C_2H_5OH. The yield of Co(HBTC)(4,4′-bipy)·3DMF was 53%

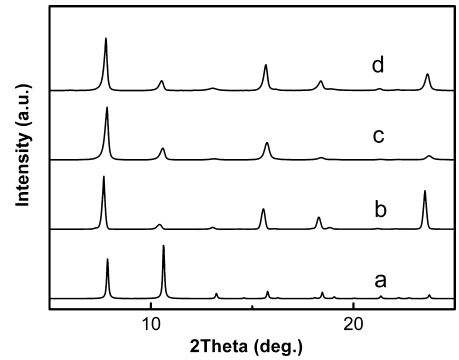

Figure 1. XRD patterns of (a) the simulation, (b) the as-synthesized sample, (c) the guest-free sample evacuated at 453 K for 2 h, and (d) the regenerated sample in DMF for Ni(HBTC)(4,4′-bipy)·3DMF.

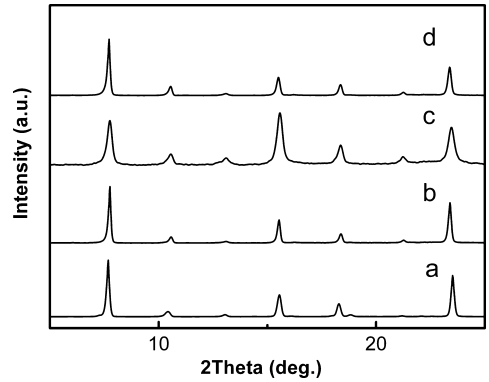

Figure 2. XRD patterns of (a) the as-synthesized sample for Ni(HBTC)(4,4′-bipy)·3DMF, (b) the as-synthesized sample for Co(HBTC)(4,4′-bipy)·3DMF, (c) the guest-free sample evacuated at 433 K for 2 h, and (d) the regenerated sample in DMF for Co(HBTC)(4,4′-bipy)·3DMF.

Thermogravimetric analysis (TGA) was carried out on a thermal analysis TGA-DSC-DTA (Q600 SDT) with a heating rate of 5 K/min under a N_2 atmosphere. Powder X-ray diffraction (XRD) tests were taken on a Rigaku D/Max2500 VB2+PC with monochromatic Cu Kα radiation to characterize the structure of the samples.

After M(HBTC)(4,4′-bipy)·3DMF was heated and evacuated for 2 h, the isotherm of nitrogen adsorption was measured on a COULTER SA 3100 apparatus at 77 K. Hydrogen storage property analysis was performed with a pressure−content−temperature measuring system, based on the volumetric method. Before each hydrogen storage test, hydrogen leaking in the equipment was checked by charging hydrogen into the equipment to reach 7.00 MPa, and a pressure change of less than 0.003 MPa over 12 h was confirmed. In addition to that, to get effective and reliable data for hydrogen uptake, the amounts of gas adsorbed in the container with MOFs and nonporous solids were compared. The background values obtained from nonporous samples were deducted from the measured original capacities.

Results and Discussion

XRD Patterns. Figures 1 and 2 provide the powder XRD patterns of the obtained M(HBTC)(4,4′-bipy)·3DMF (M = Ni and Co). The 2θ value of the peaks in the powder XRD patterns of Ni(HBTC)(4,4′-bipy)·3DMF are in agreement with the simulation. These results demonstrate the success

(10) Rosi, N. L.; Eckert, J.; Eddaoudi, M.; Vodak, D. T.; Kim, J.; O'Keeffe, M.; Yaghi, O. M. *Science* **2003**, *300*, 1127–1129.
(11) Yang, Q. Y.; Zhong, C. L. *J. Phys. Chem. B* **2006**, *110*, 655–658.
(12) Sun, D. F.; Ma, S. Q.; Ke, Y. X.; Collins, D. J.; Zhou, H. C. *J. Am. Chem. Soc.* **2006**, *128*, 3896–3897.
(13) Yang, Q. Y.; Zhong, C. L. *J. Phys. Chem. B* **2005**, *109*, 11862–11864.
(14) Collins, D. J.; Zhou, H. C. *J. Mater. Chem.* **2007**, *17*, 3154–3160.
(15) Noro, S.; Kitaura, R.; Kondo, M.; Kitagawa, S.; Ishii, T.; Matsuzaka, H.; Yamashita, M. *J. Am. Chem. Soc.* **2002**, *124*, 2568–2583.
(16) Kitagawa, S.; Kitaura, R.; Noro, S. *Angew. Chem., Int. Ed.* **2004**, *43*, 2334–2375.
(17) Seo, J. S.; Whang, D.; Lee, H.; Jun, S. I.; Oh, J.; Jeon, Y. J.; Kim, K. *Nature* **2000**, *404*, 982–986.
(18) Janiak, C. *Dalton Trans.* **2003**, 2781–2804.
(19) Chen, B. L.; Ma, S. Q.; Zapata, F.; Fronczek, F. R.; Lobkovsky, E. B.; Zhou, H. C. *Inorg. Chem.* **2007**, *46*, 1233–1236.
(20) Lin, X.; Jia, J. H.; Hubberstey, P.; Schroder, M.; Champness, N. R. *CrystEngComm* **2007**, *9*, 438–448.
(21) Habib, H. A.; Sanchiz, J.; Janiak, C. *Dalton Trans.* **2008**, 1734–1744.
(22) Braga, D.; Brammer, L.; Champness, N. R. *CrystEngComm* **2005**, *7*, 1–19.
(23) Chun, H.; Dybtsev, D. N.; Kim, H.; Kim, K. *Chem.—Eur. J.* **2005**, *11*, 3521–3529.
(24) Chapman, K. W.; Chupas, P. J.; Maxey, E. R.; Richardson, J. W. *Chem. Commun.* **2006**, 4013–4015.
(25) Gao, C. Y.; Liu, S. X.; Xie, L. H.; Ren, Y. H.; Cao, J. F.; Sun, C. Y. *CrystEngComm* **2007**, *9*, 545–547.

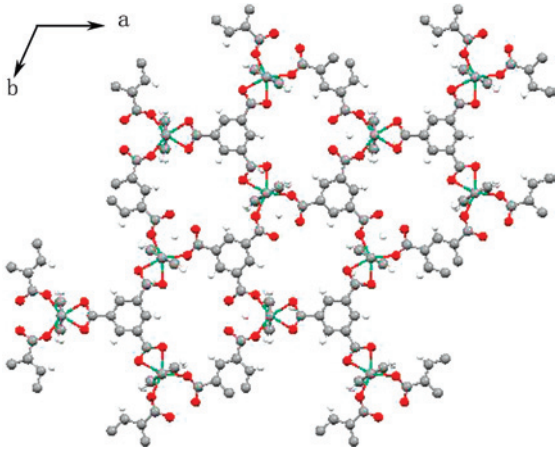

Figure 3. Paking diagram viewed along the *c* axis in Ni(HBTC)(4,4′-bipy). Ni, green; O, red; C, black; H, white.

of the synthesis. To form the framework assembled by octahedral M^{2+} centers and two kinds of connecting ligands, one of the bridging ligands (HBTC) possesses a −2 charge; the other (4,4′-bipy) should be neutral. M^{2+} ions (M = Ni and Co), bridged by $HBTC^{2-}$ divalent ions, form 2D sheets. In these 2D sheets, one of the BTC units is in bidentate mode, while the other two units are in a monodentate fasion. The sheets are further pillared by 4,4′-bipyridine along the *c* axis to form the porous structure. Following the pillaring strategy, two-dimensional grids supported by appropriate pillars (4,4′-bipy) construct a stable porous structure. Two kinds of channels exist in the porous framework of M(HBTC)(4,4′-bipy)·3DMF. One is normal rectangle channels running along the *a* and *b* axes, and the other is exceptional honeycomb channels generated by M(HBTC) layers. The peaks of Co(HBTC)(4,4′-bipy)·3DMF shift to a slightly lower angle than the ones of Ni(HBTC)(4,4′-bipy)·3DMF (Figure S1, Supporting Information). The XRD result is in accordance with the prediction because the unit cell parameters increase with the radii of M^{2+} ions, and the diffraction peaks shift to a low angle according to the Bragg equation.

For a better comparison, the XRD patterns of the evacuated sample (Figures 1c and 2c) and regenerated samples (Figures 1d and 2d) are also investigated. The results demonstrate that the crystallinity of the MOF structure remains unchanged under the given pressure and temperature conditions during gas adsorption tests.

At present, the common solvothermal methods are widely used in preparing processes of MOFs.[26−33] It is difficult to control the reaction process, investigate the mechanism, adjust the reacting time, and increase the quantity of products for closed solvothermal systems. In addition, it requires a rather long reacting time. In this paper, the compound of Ni(HBTC)(4,4′-bipy)·3DMF is synthesized by a one-pot solution assembly reaction of $Ni(NO_3)_2·6H_2O$ with the corresponding organic linkers at 393 K for only 4 h as green crystals. By using a one-pot solution method for Ni(HBTC)(4,4′-bipy)·3DMF, the reaction of crystal formation is monitored visually, and the quantity of the reactants can be simply adjusted.

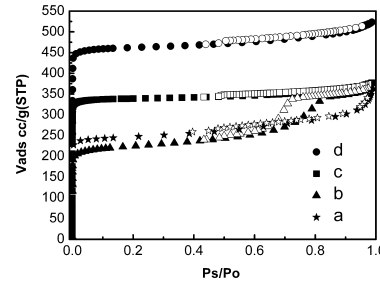

Figure 4. (a) N_2 isotherms for Co(HBTC)(4,4′-bipy)·3DMF evacuated at 433 K for 2 h at 77 K. N_2 isotherms for Ni(HBTC)(4,4′-bipy)·3DMF at 77 K after different solvent-removal treatments: (b) evacuated at 483 K for 2 h, (c) evacuated at 423 K for 2 h, and (d) evacuated at 453 K for 2 h. The shaded symbols represent adsorption, and the open symbols represent desorption.

The coordinating ability of Co^{2+} to the ligands is smaller than that of Ni^{2+}. It is beneficial for crystal formation in a solvothermal system. For the Ni^{2+} compound, the one-pot solution method seems to be a favorable choice, while for the Co^{2+} compound, which is first synthesized in this work, the solvothermal synthesis appears to be the proper process to get powders with much better crystallization and larger specific surface area than the one-pot solution reaction. Therefore, the difference of coordinating ability of metal ions leads to differences in the proper synthesis method and the crystallization of the as-prepared sample.

TGA and BET Analysis. To obtain more information about the porous structure, nitrogen adsorptions have been tested at 77 K, and the curves are shown in Figure 4. The activation for removing the guest molecules from the pores by heating under a vacuum is a required pretreatment before gas adsorption tests. The N_2 adsorption isotherms of Ni(HBTC)(4,4′-bipy)·3DMF evacuated for 2 h at 423 K (Figure 4c) and at 453 K (Figure 4d) show typically type-□ sorption behaviors, which are characteristic for the microporous structure. According to the Brunauer−Emmett−Teller (BET) equation, the specific surface areas are 1171 m^2/g for the sample evacuated at 423 K and 1590 m^2/g for the sample evacuated at 453 K. When Ni(HBTC)(4,4′-bipy)·3DMF is activated at the high temperature of 483 K (Figure 4b), the specific surface area is reduced to 784 m^2/g, and the obtained N_2 isotherm shows remarkable hysteresis, which does not appear in typical type-□ sorption. Therefore, the nitrogen adsorption is dependent on the activation. In Ni(HBTC)(4,4′-bipy)·3DMF, activations at different temperatures result in remarkable differences in N_2 isotherms and the specific surface areas. The optimal activation temperature of Ni(HBTC)(4,4′-bipy)·3DMF is 453 K according to the results.

(26) Barthelet, K.; Riou, D.; Nogues, M.; Ferey, G. *Inorg. Chem.* **2003**, *42*, 1739–1743.
(27) Wei, Q.; Nieuwenhuyzen, M.; Meunier, F.; Hardacre, C.; James, S. L. *Dalton Trans.* **2004**, 1807–1811.
(28) Wan, S. Y.; Huang, Y. T.; Li, Y. Z.; Sun, W. Y. *Microporous Mesoporous Mater.* **2004**, *73*, 101–108.
(29) Moon, H. R.; Kobayashi, N.; Suh, M. P. *Inorg. Chem.* **2006**, *45*, 8672–8676.
(30) Park, H.; Britten, J. F.; Mueller, U.; Lee, J.; Li, J.; Parise, J. B. *Chem. Mater.* **2007**, *19*, 1302–1308.
(31) Su, C. Y.; Goforth, A. M.; Smith, M. D.; Pellechia, P. J.; zur Loye, H. C. *J. Am. Chem. Soc.* **2004**, *126*, 3576–3586.
(32) Wang, Y. T.; Fan, H. H.; Wang, H. Z.; Chen, X. M. *Inorg. Chem.* **2005**, *44*, 4148–4150.
(33) He, J. H.; Zhang, Y. T.; Pan, Q. H.; Yu, J. H.; Ding, H.; Xu, R. R. *Microporous Mesoporous Mater.* **2006**, *90*, 145–152.

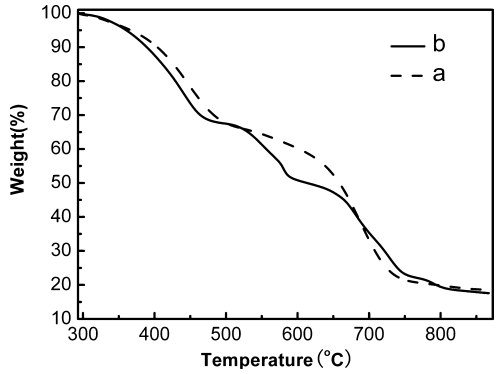

Figure 5. TGA curves of (a) Ni(HBTC)(4,4′-bipy)·3DMF (dashed) and (b) Co(HBTC)(4,4′-bipy)·3DMF (solid line).

At the lower temperature of 423 K, the solvent guest molecules could not be removed from the porous framework completely. The obtained BET surface area and corresponding pore volume are logically smaller than the actual data. However, at the higher temperature of 483 K, a partial collapse and change of the framework structure take place, which leads to the hysteresis phenomenon and relatively small surface area. In addition, the specific surface area is 1590 m^2/g for Ni(HBTC)(4,4′-bipy)·3DMF (activated at 453 K) and 887 m^2/g for Co(HBTC)(4,4′-bipy)·3DMF (activated at 433 K). The corresponding total pore volumes are 0.81 mL/g and 0.54 mL/g, respectively. Furthermore, the relatively large BET surface area (1590 m^2/g compares with 969.1 m^2/g of the solvothermally synthesized sample[25]) of Ni(HBTC)(4,4′-bipy)·3DMF reveals the advantage of the solution assembly method.

Thermogravimetric analysis (Figure 5) shows the weight loss in M(HBTC)(4,4′-bipy)·3DMF in a N_2 atmosphere. The framework of Ni(HBTC)(4,4′-bipy)·3DMF does not collapse up to 503 K. Due to the decreased coordination ability of Co^{2+}, the decomposing temperature of Co(HBTC)(4,4′-bipy)·3DMF is about 473 K. The porous structures are prepared in a DMF solution, and the pores are filled with solution molecules. The first major weight loss step (34%) corresponds to the removal of three DMF molecules from the framework (the calculated weight change for three DMF molecules per M(HBTC)(4,4′-bipy)·3DMF is 34%). The following step, in the region of high temperatures, corresponds to the decomposition of the structure.

MOFs, built up by connecting inorganic parts with various organic linkers, have an important characteristic that the porosity of the framework may not exist under high-temperature evacuation treatment. Therefore, in the research on MOFs, TGA analysis results not only show the thermal stability of MOFs but also turn out to be decisive data to ensure an optimized temperature of activation to remove the guest molecules. According to TGA data, the weight loss of Ni(HBTC)(4,4′-bipy)·3DMF is 30% (34% for three DMF molecules) at 483 K. However, during thermal and vacuum pretreatment for 2 h before gas adsorption tests, it is notable that Ni(HBTC)(4,4′-bipy)·3DMF cannot keep the entire porous framework at 483 K. The results reveal that this pretreatment is the crucial process determining the gas sorption property.

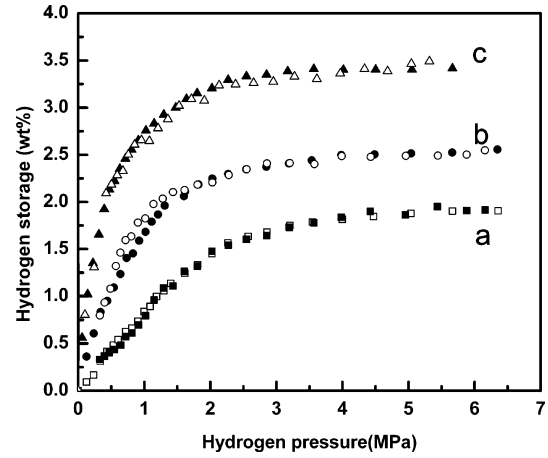

Figure 6. Hydrogen adsorption (shaded symbols) and desorption (open symbols) isotherms for Ni(HBTC)(4,4′-bipy)·3DMF at (a) 98 K, (b) 90 K, and (c) 77 K.

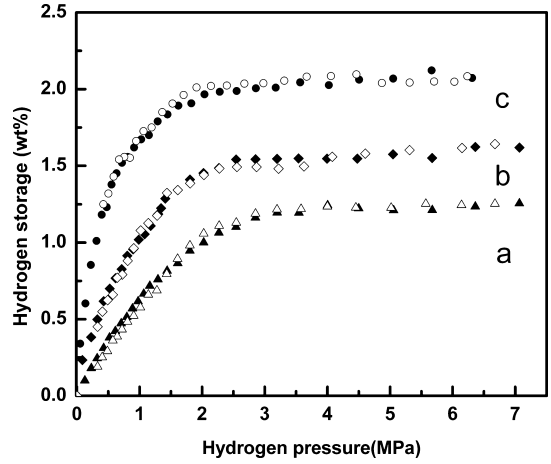

Figure 7. Hydrogen adsorption (shaded symbols) and desorption (open symbols) isotherms for Co(HBTC)(4,4′-bipy)·3DMF at (a) 98 K, (b) 90 K, and (c) 77 K.

Hydrogen Adsorption Analysis. Figures 6 and 7 present the hydrogen sorption isotherms at 77, 90, and 98 K. All isotherms show full reversibility without hysteresis. At 77 K, Ni(HBTC)(4,4′-bipy)·3DMF has a hydrogen capacity of 3.42 wt % and Co(HBTC)(4,4′-bipy)·3DMF has a saturated capacity of 2.05 wt %. The critical temperature of hydrogen is 33 K, which is lower than the experimental temperature (77 K). Due to the weak interaction between hydrogen molecules in the adsorption at supercritical temperatures, multilayer adsorption can hardly be achieved, and only a monolayer is formed. On the basis of the monolayer hypothesis, the hydrogen uptake amount on a unit specific surface area is estimated to be 2.27 wt % per 1000 m^2/g.[34,35] For M(HBTC)(4,4′-bipy)·3DMF (M = Ni and Co), the saturation values of hydrogen adsorption calculated from Figures 6 and 7 are 2.15 wt % and 2.31 wt % per 1000 m^2/g. The results are in accordance with the monolayer prediction. The shapes of isotherms for nitrogen sorption and hydrogen sorption measured both at 77 K are unlike. The saturation amount for adsorption is accomplished under the higher pressure in hydrogen adsorption (Figures 6 and 7) than in nitrogen adsorption (Figure 4) at 77 K. Nitrogen adsorption carried out below its critical temperature (126 K)

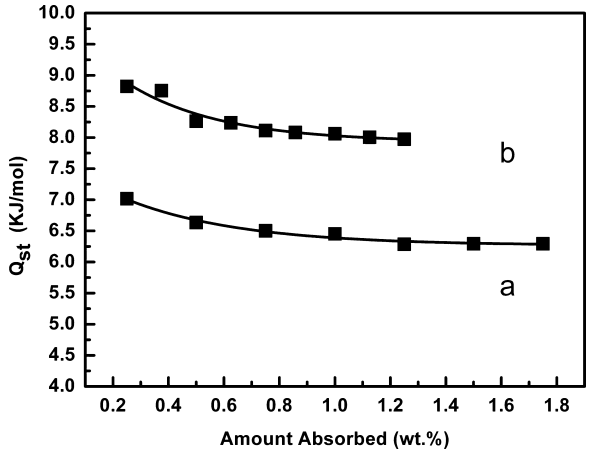

Figure 8. Coverage dependency of the heat of adsorption (Q_{st}) for H_2 in (a) Ni(HBTC)(4,4′-bipy)·3DMF and (b) Co(HBTC)(4,4′-bipy)·3DMF.

behaves differently from the supercritical adsorption of hydrogen.

To investigate the interaction between H_2 and the framework, the Clausius−Clapeyron equation, used in physical adsorption analysis,[34−37] has been adopted in the calculations of adsorption heats. To extract the coverage-dependent adsorption heat for the compound, the data measured at 77, 90, and 98 K are caculated by the equation

$$(\ln P)_n = -\frac{Q_{st}}{RT} + C$$

where P is the pressure, n is the amount adsorbed, T is the temperature, R is the universal gas constant, and C is a constant. The hydrogen adsorption heat in M(HBTC)(4,4′-bipy)·3DMF is obtained by calculating the slope of the ln P − (−1/RT) curve. The adsorption heat at the low coverage of 0.25 wt % is 7.0 kJ/mol for Ni(HBTC)(4,4′-bipy)·3DMF and 8.8 kJ/mol for Co(HBTC)(4,4′-bipy)·3DMF. In Figure 8, the heat shows a gradual decrease in value as a function of the adsorbed amount of H_2. The decrease indicates that the H_2 molecules are combined with stronger biding sites preferentially, and it is possibly attributed to different interacting sites located at different types of channels in M(HBTC)(4,4′-bipy)·3DMF.

Co(HBTC)(4,4′-bipy)·3DMF adsorbs much less hydrogen and nitrogen than Ni(HBTC)(4,4′-bipy)·3DMF, which has an identical structure to it. As mentioned above, the coordination abilities of metal ions affect the choice of suitable synthesis method. The M(HBTC)(4,4′-bipy)·3DMF prepared by the solution assembly method and that by the solvothermal method reveal different saturation capacities in gas adsorption. Depending on the preparation for M(HBTC)(4,4′-bipy)·3DMF with different metal ions, the hydrogen storage capacity varies. Furthermore, the hydrogen adsorption heat of Co(HBTC)(4,4′-bipy)·3DMF is larger

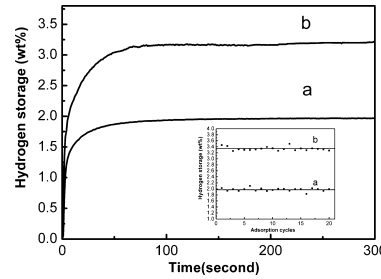

Figure 9. Kinetic trace for hydrogen adsorption of the sample on exposure to a pressure of 2.00 MPa of H_2 gas for M(HBTC)(4,4′-bipy)·3DMF [(a) M = Co^{2+} and (b) M = Ni^{2+}] at 77 K. Inset: Hydrogen storage capacity of M(HBTC)(4,4′-bipy)·3DMF [(a) M = Co^{2+} and (b) M = Ni^{2+}] measured for sequential H_2 sorption cycles.

than that of Ni(HBTC)(4,4′-bipy)·3DMF (Figure 8), and it reveals the effects of metal ions in MOFs on hydrogen adsorption. Due to the same ligands and framework structure in Co(HBTC)(4,4′-bipy)·3DMF and Ni(HBTC)(4,4′-bipy)·3DMF, the difference in adsorption heat should be attributed to the dissimilar d electronic structure of Co^{2+} and Ni^{2+}. Therefore, by adopting different metal ions, for example, Co^{2+}, the interaction between hydrogen and MOFs can be further enhanced.

For hydrogen storage materials, the key characteristics include not only hydrogen uptake capacity in the proper conditions but also the sorption rate and the reversibility.[1] Hydrogen adsorption rates given in Figure 9 reveal that, just in a short time of about 80 s, hydrogen adsorption reaches the saturation under an initial hydrogen pressure of 2.00 MPa. The rapid adsorption process, as expected for physisorption, demonstrates that the compounds can rapidly adsorb the proper capacities of 3.34 wt % and 1.97 wt % of hydrogen under a low initial pressure of 2.00 MPa. In addition, no obvious decline in hydrogen storage capacity is found after 20 sorption cycles. These illustrate that M(HBTC)(4,4′-bipy)·3DMF has favorable kinetic properties and reversibility for hydrogen storage.

Different from the results at low temperatures of 77, 90, and 98 K, M(HBTC)(4,4′-bipy)·3DMF presents a linear increasing trend on the hydrogen adsorption curve up to 1.20 wt % for Ni(HBTC)(4,4′-bipy)·3DMF and 0.96 wt % for Co(HBTC)(4,4′-bipy)·3DMF at 298 K (Figure 10). The hydrogen storage capacity is proportional to the applied pressure from 0.01 to 7.20 MPa. The slopes are 0.162 wt % per MPa and 0.133 wt % per MPa, respectively. It has been published that IRMOF-1 showed a 0.45 wt % linear hydrogen uptake under 60 bar (0.075 wt % per MPa) at 298 K and IRMOF-8 presented a capacity of 0.4 wt % at 30 bar (0.133 wt % per MPa).[40,41] Considering the smaller surface areas and lower hydrogen capacities at nitrogen temperatures of M(HBTC)(4,4′-bipy)·3DMF, it is notable that M(HBTC)(4,4′-bipy)·3DMF presents an even higher hydrogen uptake and steeper slopes of linear isotherms than those of IRMOFs at

(34) Züttel, A. *Mater. Today* **2003**, *6*, 24–33.
(35) Li, Y. W.; Liu, Y.; Wang, Y. T.; Leng, Y. H.; Xie, L.; Li, X. G. *Int. J. Hydrogen Energy* **2007**, *32*, 3411–3415.
(36) Lin, X.; Jia, J. H.; Hubberstey, P.; Schroder, M.; Champness, N. R. *CrystEngComm* **2007**, *9*, 438–448.
(37) Krungleviciute, V.; Lask, K.; Heroux, L.; Migone, A. D.; Lee, J. Y.; Li, J.; Skoulidas, A. *Langmuir* **2007**, *23*, 3106–3109.
(38) Li, Y.; Yang, R. T. *Langmuir* **2007**, *23*, 12937–12944.
(39) Zhou, W.; Wu, H.; Hartman, M. R.; Yildirim, T. *J. Phys. Chem. C* **2007**, *111*, 16131–16137.
(40) Rowsell, J. L. C.; Yaghi, O. M. *J. Am. Chem. Soc.* **2006**, *128*, 1304–1315.
(41) Dailly, A.; Vajo, J. J.; Ahn, C. C. *J. Phys. Chem. B* **2006**, *110*, 1099–1101.

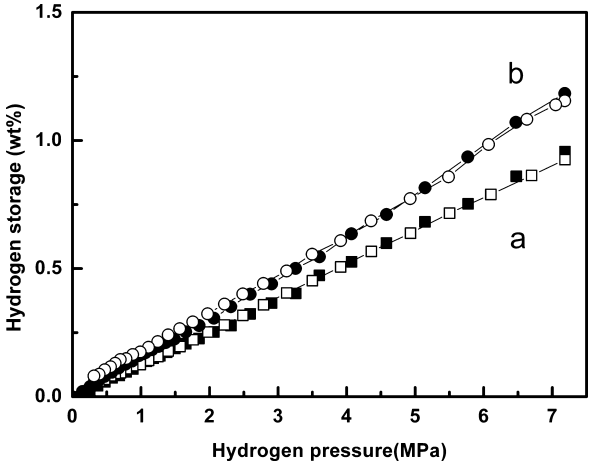

Figure 10. Hydrogen adsorption (shaded symbols) and desorption (open symbols) isotherms for M(HBTC)(4,4′-bipy)·3DMF [(a) M = Co^{2+} and (b) M = Ni^{2+}] at 298 K.

298 K. The high capacities of M(HBTC)(4,4′-bipy)·3DMF at 298 K are probably attributed to its specific framework. Compared to the common rectangle channels in IRMOFs, the honeycomb-like channels with a rolling surface in M(HBTC)(4,4′-bipy)·3DMF should affect the interaction of adsorbent and hydrogen and increase the hydrogen adsorption properties at room temperature. In addition, no saturation is observed at room temperature in Figure 10, and this phenomenon is consistent with previous reports.[5,6,10,40,41] A recent study[44] has proved that, in MOFs with a relatively large pore volume, hydrogen would reach saturation pore filling only at sufficiently high pressures. M(HBTC)(4,4′-bipy)·3DMF exhibits the most favorable values of capacity reported so far for hydrogen physisorption at room temperature. It has been proposed that, for physisorption materials, the optimum value of adsorption enthalpy for maximum hydrogen delivery should be −15.1 kJ/mol.[45] Considering the adsorption heats of M(HBTC)(4,4′-bipy)·3DMF, which are about 7.0 and 8.8 kJ/mol for each compound (Figure 8), it is possible to further increase the capacities of hydrogen at room temperature by adopting other metal ions or ligands to enhance the adsorption heats.

Although large pore volumes and surface areas are significant factors for the physisorption of hydrogen,[43] it is obviously difficult to create a MOF with an extremely large surface area and pore volume because of Aristotle's observation that "nature abhors a vacuum". Various studies have indicated that the smaller pores and channels actually take up hydrogen more effectively than the larger ones.[35,43] Meanwhile, researchers have proposed that the nonlinearity of the framework has also been a factor in determining hydrogen uptake.[14,23,24] The M(HBTC)(4,4′-bipy)·3DMF contains nonlinear honeycomb channels with only 5 Å at the narrowest and 8 Å at the widest spacing and rectangle channels with the size of 7 Å × 6 Å.[25] The channel sizes in M(HBTC)(4,4′-bipy)·3DMF are appropriate for hydrogen molecules with a van der Waals diameter of 2.4 Å to enter the porous structure and be adsorbed. Considering the organic ligands (H_3BTC, bipy) and the framework structure, it is notable that the entire surface exposed to gas is the electron cloud of ν bands. The interaction of ν bands with hydrogen molecules might contribute to the adsorption.[35] Furthermore, the specific rolling surface of the channels with the appropriate size for hydrogen sorption should induce a high capacity of hydrogen. The nonlinear honeycomb channels may contribute to the interaction between adsorbent and hydrogen molecules, which is significant for increasing the hydrogen capacity of MOFs at ambient temperatures.

Conclusion

In conclusion, Ni(HBTC)(4,4′-bipy)·3DMF has been successfully synthesized by the mild solution assembly reaction, and Co(HBTC)(4,4′-bipy)·3DMF has been first synthesized by the solvothermal method. Both the surface area and the quantity of Ni(HBTC)(4,4′-bipy)·3DMF can be increased by monitoring the solution assembly process. In Ni(HBTC)(4,4′-bipy)·3DMF, the activation process shows distinct effects on the exposed surface areas and pore volumes and is the key step for hydrogen storage. The optimal activation temperature is 453 and 433 K for M(HBTC)(4,4′-bipy)·3DMF (M = Ni and Co), respectively. M(HBTC)(4,4′-bipy)·3DMF (M = Ni and Co) shows favorable H_2 uptake at room temperature (1.20 wt % and 0.96 wt % under 7.20 MPa) and 77 K (3.42 wt % and 2.05 wt %). In kinetic research, the MOFs exhibit a short loading time for hydrogen upload and favorable reversibility at 77 K. By adopting the Clausius−Clapeyron equation, the heat values of hydrogen adsorption are calculated and show a gradual decrease as a function of the adsorbed hydrogen. The interaction between H_2 and M(HBTC)(4,4′-bipy)·3DMF shows a preferential trend. The favorable hydrogen storage properties are attributed to the special structure, which contains rolling honeycomb-like and rectangle channels with an appropriate size for hydrogen uptake. Furthermore, it is reasonable to suggest that, for efficient hydrogen storage, the idealized porous MOFs not only should have the proper pore size and chemical nature but should also contain the appropriate surface and nonlinearity that best match the H_2 molecules to compact interactions with the porous surface.

Acknowledgment. The authors acknowledge the National Natural Science Foundation of China (Nos. 20221101 and 20671004), MOST of China (Nos. 2006AA05Z130, 2007AA05Z118), and MOE of China (No. 707002).

Supporting Information Available: Additional figures. This material is available free of charge via the Internet at http://pubs.acs.org.

IC800919K

(42) Fang, Q. R.; Zhu, G. S.; Xue, M.; Zhang, Q. L.; Sun, J. Y.; Guo, X. D.; Qiu, S. L.; Xu, S. T.; Wang, P.; Wang, D. J.; Wei, Y. *Chem.—Eur. J.* **2006**, *12*, 3754–3758.
(43) Banu Kanli, Y. C. M. R. S. E. B. B. C. B. W. L. *Angew. Chem., Int. Ed.* **2005**, *44*, 72–75.
(44) Skoulidas, A. I.; Sholl, D. S. *J. Phys. Chem. B* **2005**, *109*, 15760–15768.
(45) van den Berg, A. W. C.; Arean, C. O. *Chem. Commun.* **2008**, 668–681.